Materials Letters 166 (2016) 140–144

Contents lists available at ScienceDirect

Materials Letters

journal homepage: www.elsevier.com/locate/matlet

# Multi-scale architectured thermoelectric materials in the $Mg_2(Si,Sn)$ system

S. Gorsse [a,b,c,*], S. Vivès [b,c], P. Bellanger [b,c], D. Riou [a,c], L. Laversenne [d,e,f], S. Miraglia [e,f], D.R. Clarke [d]

[a] Bordeaux INP, ICMCB, UPR 9048, 33600 Pessac, France
[b] CNRS, ICMCB, UPR 9048, 33600 Pessac, France
[c] Univ. Bordeaux, ICMCB, UPR 9048, 33600 Pessac, France
[d] School of Engineering and Applied Sciences, Harvard University, Cambridge, MA, USA
[e] CNRS, Inst NEEL, F-38000 Grenoble, France
[f] Univ. Grenoble Alpes, Inst NEEL, F-38000 Grenoble, France

ARTICLE INFO

*Article history:*
Received 20 October 2015
Received in revised form
9 December 2015
Accepted 12 December 2015
Available online 14 December 2015

*Keywords:*
Solidification microstructure
Thermoelectric materials
Mesostructure
Thermodynamics

ABSTRACT

Two different microstructural architectures featuring multiple length scales have been created in the thermoelectric $Mg_2(Si_xSn_{1-x})$ system. The first one combines the nano-grain microstructure, characteristic of rapid solidification, with a large-scale pseudo-periodic pattern in one direction. The second is a layered structure in which the composition and microstructural scale vary from layer to layer. The microstructural variability is obtained by two different processing methods, in the first from the consolidation of melt-spun $Mg_2(Si_xSn_{1-x})$ alloy and in the second the sequential thermal treatment of a diffusion couple between $Mg_2Si$ and $Mg_2Sn$. In both cases the microstructural features are consistent with the predictions of the solidification and diffusion paths followed in each process.



## 1. Introduction

Thermoelectric generators (TEGs) convert heat directly into usable electric power. As huge amounts of heat are wasted or unutilized from a wide variety of sources, ranging from industrial activities to automobile engines, there is continued interest in developing TEGs. Unfortunately, at present, the energy conversion efficiencies of these devices is too low for many practical applications and so the thrust of much of the materials development is in increasing the efficiency expressed in terms of the material figure of merit, ZT. For a chemically and spatially homogeneous material, such as any of the common materials, including the magnesium silicides and its alloys, maximizing the figure of merit requires maximizing an unusual combination of properties: electrical conductivity, Seebeck coefficient as well as thermal resistivity. In recent years, much of the development of materials with enhanced values of ZT has been to create, by microstructural processing, nano-structural features that increase phonon scattering to lower the lattice thermal conductivity [1–7]. However, the presence of nanometer-scale defects such as nano-sized precipitates, affect only a portion of the phonon spectrum, typically those with small mean free paths, and phonons with longer mean free paths remain unaffected. Indeed, in many semiconductors, even phonons with mean free path above 100 nm can significantly contribute to heat conduction [8]. Consistent with this is the observation that a further reduction of the thermal conductivity can be achieved by introducing meso-scale defects to scatter the phonons with longer mean free paths [4]. Moreover, while the focus in these recent studies has been to decrease thermal conductivity, it has been implicitly assumed that the power factor is relatively unaffected. Of wider interest is the possibility that an initially homogeneous material can be converted into a deliberately architectured material of the same overall composition to not only decrease thermal conductivity by introducing phonon scattering at different length scales but also to modify other important properties, such as the fracture toughness. Inevitably, an architectured thermoelectric will be a composite thermoelectric rather than a homogeneous material and consequently ZT will be related to the phases through some mixing rules of the thermoelectric properties of the individual phases. It is also possible but not investigated in thermoelectric systems that some of the metastable compositions may have superior TE properties to those of the equilibrium solid solution phases.

Motivated by the desire to create materials with multiple microstructural length scales, we have been exploring processing

* Corresponding author at: Bordeaux INP, ICMCB, UPR 9048, 33600 Pessac, France.
*E-mail address:* gorsse@icmcb-bordeaux.cnrs.fr (S. Gorsse).

http://dx.doi.org/10.1016/j.matlet.2015.12.056
0167-577X/

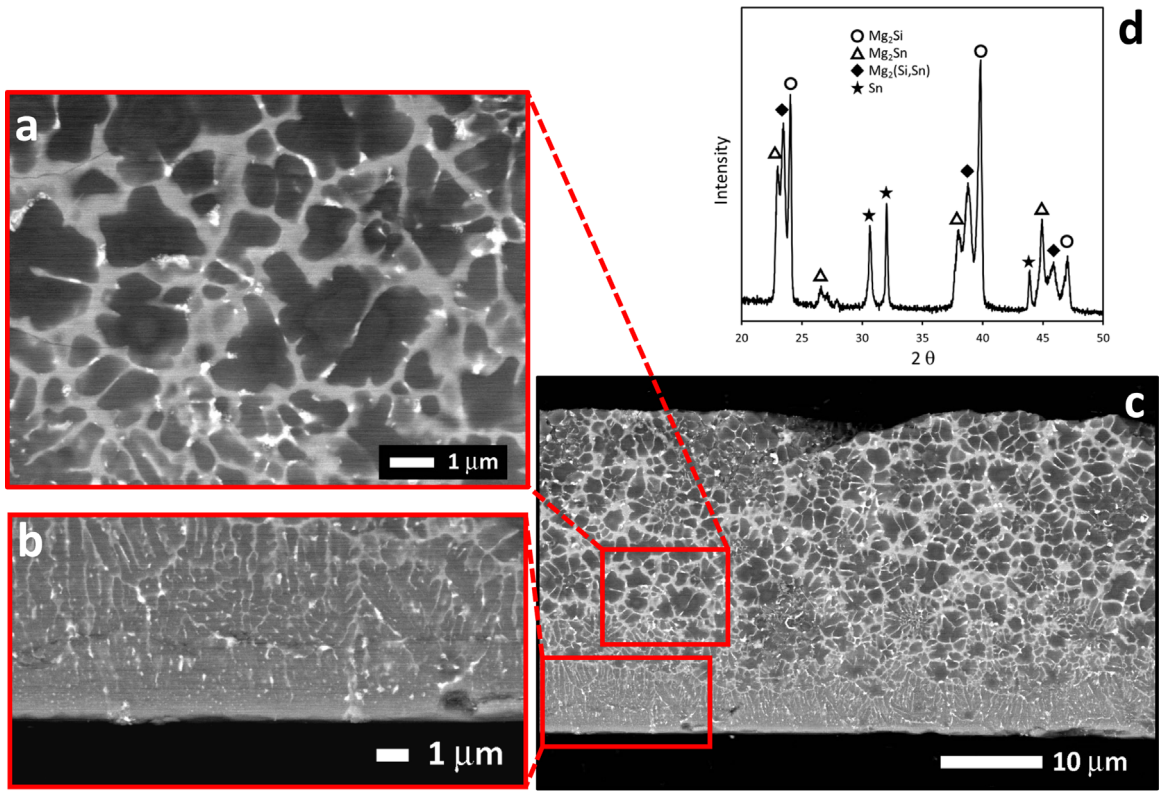


**Fig. 1.** (a–c) SEM-BSE images showing the graded microstructure of the $Mg_2Si_{0.65}Sn_{0.35}$ melt-spun ribbons. (d) XRD diagram of the melt-spun $Mg_2Si_{0.65}Sn_{0.35}$ ribbons.

routes to produce a variety of architectured thermoelectric materials. In the area of structural materials, Bouaziz et al. [9] have recently outlined approaches to also introduce intermediate length scales between the microstructure and the superstructures in order to provide additional degrees of freedom in manipulating property combinations hitherto unattainable [10–12]. A few examples can be found for functional materials such as Cu/Nb nanowires, which simultaneously have both high strength and high electrical conductivity [13], or segmented TE to increase the overall conversion efficiency in TEG by stacking materials with different peak temperatures of the figure of merit [14].

In the present work, we demonstrate the formation of $Mg_2(Si, Sn)$ thermoelectric materials having two different types of microstructural architectures. The first is one that combines the nano-grain microstructure, characteristic of rapid solidification with a large-scale pseudo-periodic pattern in one direction. The second is a layered structure in which the composition and microstructural scale vary in each layer. The $Mg_2(Si_xSn_{1-x})$ alloy system was chosen for illustration because it can be cast from the melt, exhibits a range of solid solution compositions that have been shown to be promising thermoelectric materials, and the binary phases are also thermoelectric.

## 2. Experimental

For the formation of the first architecture, alloys having compositions of $Mg_2Si$ and $Mg_2Si_{0.65}Sn_{0.35}$ were prepared by induction melting of magnesium (99.9%), silicon (99.999%) and tin (99.999%) sealed in a tantalum crucible under a low pressure argon atmosphere in order to minimize evaporation and oxidation. After solidifying, the ingots produced were melted in boron nitride (BN) crucibles and then melt-spun onto a copper wheel spinning at a speed of 30 m/s to form rapidly-solidified ribbons a few tens of micrometers in thickness. These ribbons were then stacked in a graphite die and consolidated by spark plasma sintering at 70 MPa, 500 °C for 5 min to form a dense, pseudo-periodic, graded microstructure. Comparison samples were produced in the same way but instead of stacking the ribbons, they were first crushed before consolidation.

An alternative architecture is a one-dimensional stepped variation in composition and structure. This was formed by creating a diffusion couple between a $Mg_2Si$ and a $Mg_2Sn$ pellet [15] and then annealed at successively higher temperatures. Ingots of the pure phases $Mg_2Si$ and $Mg_2Sn$ were prepared by induction melting as described in the previous section. After cooling, they were ground before consolidating by spark plasma sintering (SPS) to produce highly dense polycrystalline pellets of 10 mm diameter. Prior to the bonding process, the pellets faces were finely polished. Successful bonding of the two pellets occurred within 1 h at 600 °C under a moderate pressure of 60 MPa. The diffusion couples obtained this way were placed into Ta tubes, sealed under argon and then successively heated at 600, 500 and 400 °C for 3.5 h, 23 h and 109 h, respectively, conditions chosen in this particular example to develop inter-diffusion layers having different microstructures with similar thicknesses.

## 3. Results and discussion

The hierarchical microstructure of the melt-spun ribbons is shown in the SEM images of polished cross-sections of Fig. 1a–c. In the electron back scatter imaging mode used, the darkest phase in the images has the lowest mean atomic number and, by EDAX, is associated with $Mg_2Si$. The $Mg_2Si$ ribbons consist of $Mg_2Si$ grains surrounded by a fine eutectic structure of $Mg_2Si+Si$. The size and shape of the $Mg_2Si$ grains vary across the thickness of the ribbon varying from thin grains elongated along the thermal gradient in contact with the copper wheel to equiaxed grains on the free surface of the ribbon. This gradient of microstructure indicates

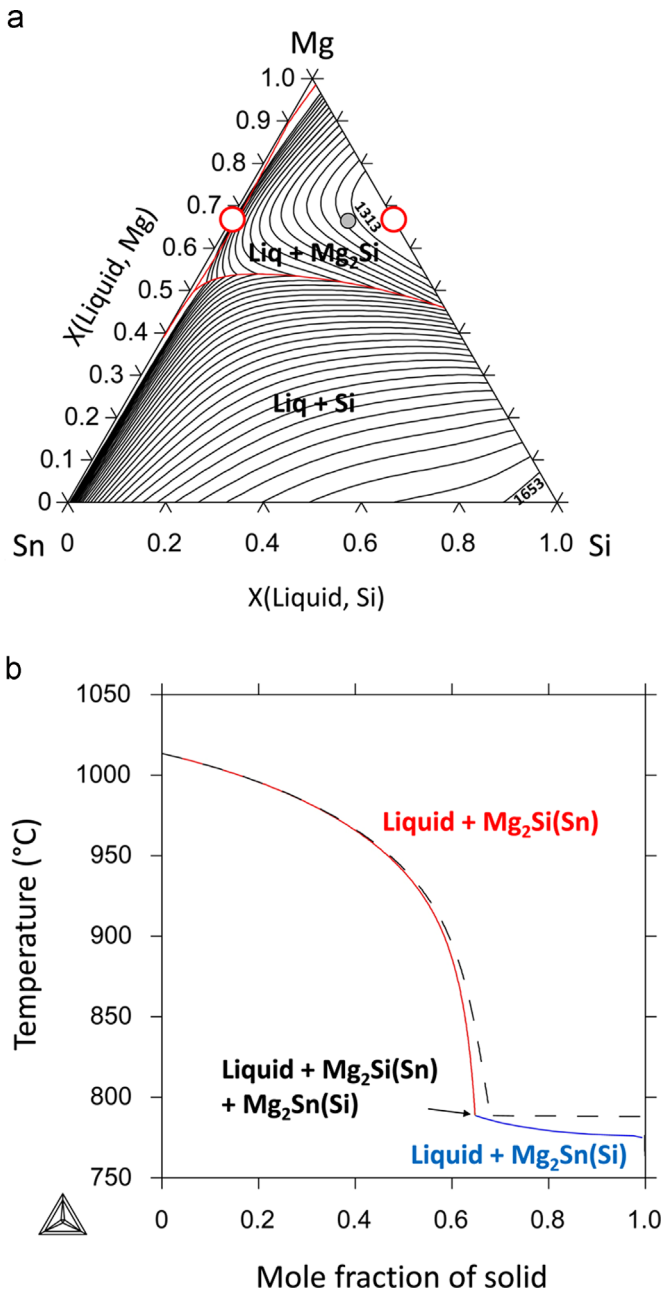


**Fig. 2.** (a) The calculated Mg–Si–Sn liquidus surface. Isotherms are represented every 20 K. The red lines indicate uni-variant reactions. The red dots stand for $Mg_2Si$ and $Mg_2Sn$ phases. The gray dot shows the $Mg_2Si_{0.65}Sn_{0.35}$ alloy composition. (b) Solid fraction vs temperature for the $Mg_2Si_{0.65}Sn_{0.35}$ alloy from the Scheil–Gulliver simulation.(For interpretation of the references to color in this figure legend, the reader is referred to the web version of this article.)

that the melt-spinning process involves a significant gradient of cooling rate. This also strongly affects the microstructure of the $Mg_2Si_{0.65}Sn_{0.35}$ melt-spun ribbons, as shown in Fig. 1a–c. XRD diffraction (Fig. 1d) indicates that the microstructure is composed of the two end member compounds, $Mg_2Si$ and $Mg_2Sn$, a $Mg_2(Si, Sn)$ solid solution as well as a small amount of isolated, pure Sn particles. On the copper wheel side of the ribbon (Fig. 1b), the columnar area is mainly composed of $Mg_2(Si,Sn)$, which EPMA indicates has the nominal composition of the sample $Mg_2Si_{0.65}Sn_{0.35}$. According the phase diagram [16–18], this composition is a metastable supersaturated solid solution that lies within the miscibility gap indicating that its formation is a result of the very high cooling rate the melt would have experienced when in contact with the copper wheel. The high cooling rate prevents partitioning of the solute atoms leading to polymorphous solidification. On the other side of the ribbon, where the cooling rates are lower, partitioning occurs and results in the formation of $Mg_2Si$-rich dendrites surrounded by a $Mg_2Sn$-rich matrix. The formation of these phases during cooling is consistent with the calculated liquidus surface (Fig. 2a) and the Scheil–Gulliver simulation (Fig. 2b) performed using ThermoCalc and the thermodynamic assessment from Kozlov et al. [19]. Only the presence of pure Sn differs from the predictions of the calculations and presumably occurs due to a loss Mg by volatilization whilst the alloy was molten.

Fig. 3b illustrates the microstructure obtained after SPS consolidation of the stacked ribbons. Under the consolidation conditions used, the fine and graded microstructure of the individual ribbons is preserved. Moreover, there is a periodically graded structure through the bulk consisting of alternating single-phase layers of supersaturated $Mg_2(Si,Sn)$ solid solution with two-phase layers consisting of $Mg_2Si$-rich dendrites embedded in a continuous $Mg_2Sn$-rich matrix phase. For comparison, Fig. 3a illustrates the alloy in its as-cast condition. In addition to the microstructural features observed in the as-spun alloy (quenched ribbon) - i.e. primary $Mg_2Si(Sn)$ dendrites, $Mg_2Sn(Si)$ matrix and particles of pure Sn -, one can note the formation of an outer shell that surrounds the $Mg_2Si(Sn)$ dendrites. This is the result of the peritectic reaction: primary crystallites undergoing peritectic reaction with liquid to form an envelope of $Mg_2Sn(Si)$ being of peritectic composition, whereas the surrounded $Mg_2Sn(Si)$ matrix, depleted in Si, is formed at temperature below that of the peritectic reaction. The microstructure is consistent with the phase existence fields, as well as the invariant reactions, in the $Mg_2Si$-$Mg_2Sn$ quasi-binary phase diagram as proposed in the literature [16–18].

Fig. 4a shows the images of the reaction zones formed between the $Mg_2Si/Mg_2Sn$ diffusion couples. It was found, as illustrated in the figure, that different layers were formed, the first at 400 °C, the second at 500 °C and the third at 600 °C. The three layers are: (i) a single-phase layer of the $Mg_2(Si,Sn)$ solid solution exhibiting concentration gradients in Si and Sn in direct contact with the unaffected $Mg_2Sn$ end member, (ii) a layer of a two-phase of $Mg_2Sn$ and pure Si having a coarse microstructure, and (iii) in contact with $Mg_2Si$, the same two-phase layer but with a finer microstructure. This sequence of layers indicates that the diffusion paths are different at the three temperatures, consistent with Kirkaldy's rule [20] namely that the diffusion path is a line in the phase diagram that begins at the composition of one end-member of the diffusion couple, crosses phase fields involved in the formation of the sequence of intermediate layers, and ends at the other end-member. Invoking this rule, it is possible to describe the diffusion path tracking the composition changes across the inter-diffusion zone in concordance with the phase diagram (Fig. 4b). At 400 °C and 500 °C the diffusion path crosses tie-lines in the $Mg_2Sn+Si$ two-phase field which represents the formation of a two-phase layer in the inter-diffusion zone, then it crosses a three-phase field corresponding to the interphase with equilibrium between three phases: $Mg_2Sn$, $Mg_2Si$ and Si. At 600 °C, the diffusion path crosses only a single phase field which corresponds to the single-phase layer $Mg_2(Si,Sn)$ in the inter-diffusion zone, then it crosses a two-phase field along a tie-line in the quasi-binary $Mg_2Sn$–$Mg_2Si$ system, corresponding to the interface with equilibrium between two phases: $Mg_2Sn(Si)$ and $Mg_2Si(Sn)$.

## 4. Conclusion

In summary, we have demonstrated that it is possible to create two quite different architectured microstructures from a solid-

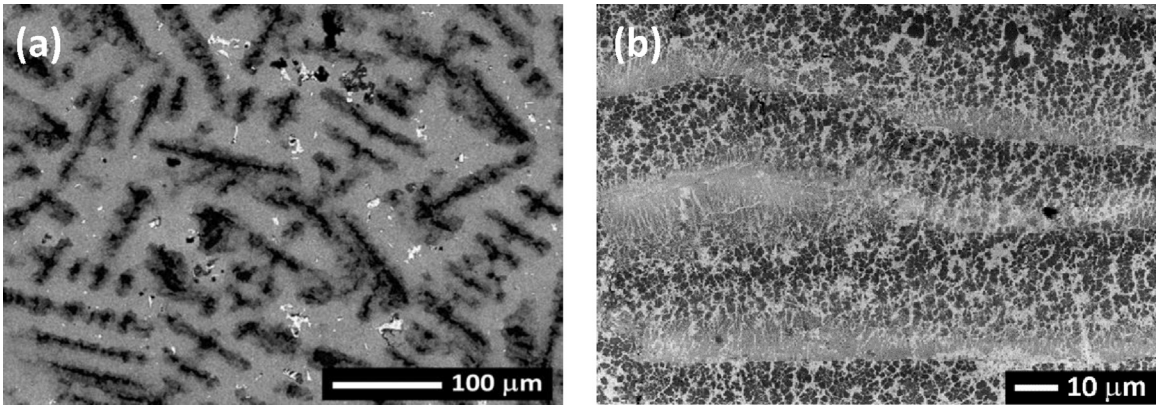


**Fig. 3.** (a) The microstructure of the slowly-cooled, as-cast $Mg_2Si_{0.65}Sn_{0.35}$ ingot. (b) The pseudo-periodic graded microstructure of the $Mg_2Si_{0.65}Sn_{0.35}$ after sintering of the stacked ribbons. The stacking is horizontal in this image. SEM-BSE images.

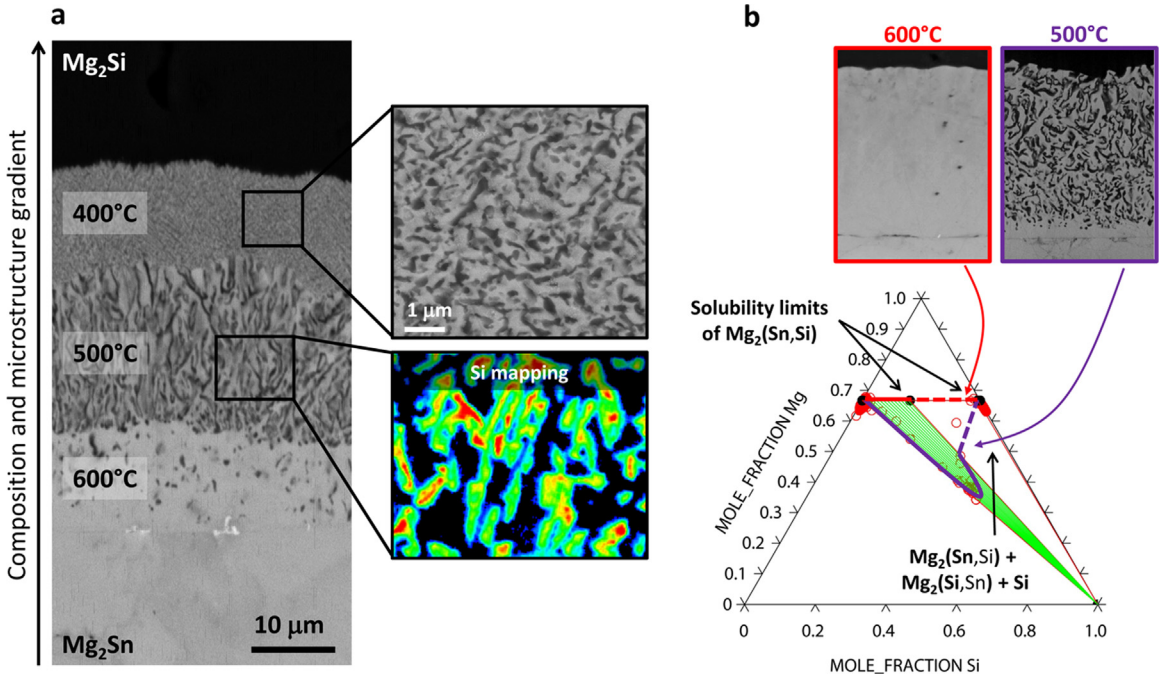


**Fig. 4.** (a) Graded layered microstructure produced by the diffusion couple at the indicated temperatures (Polishing was carried out in ethanol to avoid oxidation of the magnesium.), and (b) diffusion paths represented in the isothermal section of the Mg–Si–Sn ternary phase diagram.

solution quasi-binary alloy by using a combination of standard metallurgical processing procedures. In the first example the architecturing results from a two-step process combining the advantages of rapid solidification to form a nanostructured microstructure in thin sheets with spark plasma sintering to quickly consolidate without appreciable microstructural coarsening, to create a structure that also has a substantially larger structural pseudo-periodicity with an internal gradient. The second example uses multi-step solid-state inter-diffusion to create a layered architecture in which each layer has a different microstructural scale. In both examples, the different structures formed are a result of kinetic limitations during processing and, as illustrated, their phase compositions can be readily interpreted by thermodynamic assessment of the ternary Mg–Sn–Si system. Based on these exploratory findings, it should be feasible – to the extent allowed by the underlying thermodynamics – to refine the processes, and their sequence, to tailor the scales of the architectured microstructures for a wide variety of inter-metallic alloys. There are many challenges, for instance determining the distribution coefficients of dopants, in exploiting these approaches in developing $Mg_2(Si,Sn)$ alloys with improved thermoelectric properties but the sequential inter-diffusion process may, for instance, be a viable method of making graded electrical contacts as well as creating, in-situ a segmented thermoelectric.

## Acknowledgments

L.L. wishes to thank Région Rhône-Alpes (CMIRA grant 14.004457) and French Ministry of Defence (DGA – ERE grant 2014.60.0080) for financial support.

## References

[1] Y. Lan, A.J. Minnich, G. Chen, Z. Ren, Adv. Funct. Mater. 20 (2010) 357.
[2] S. Gorsse, P. Bellanger, Y. Brechet, E. Sellier, A. Umarji, U. Ail, R. Decourt, Acta Mater. 59 (2011) 7425.
[3] S. Gorsse, P.B. Pereira, R. Decourt, E. Sellier, Chem. Mater. 22 (2010) 988.
[4] K. Biswas, J. He, I.D. Blum, C.I. Wu, T.P. Hogan, D.N. Seidman, V.P. Dravid, M. G. Kanatzidis, Nature 489 (2012) 414.
[5] G.J. Snyder, E.S. Toberer, Nat. Mater. 7 (2008) 105–114.

[6] N.A. Heinz, T. Ikeda, Y. Pei, G.J. Snyder, Adv. Funct. Mater. 24 (2014) 2135.
[7] P. Bellanger, S. Gorsse, S. Vivès, G. Bernard-Granger, C. Navone, A. Redjaimia, Acta Mater. 95 (2015) 102.
[8] B. Qiu, H. Bao, G. Zhang, Y. Wu, X. Ruan, Comput. Mater. Sci. 53 (2012) 278.
[9] O. Bouaziz, Y. Brechet, J.D. Embury, Adv. Eng. Mater. 10 (2008) 24.
[10] M.F. Ashby, Acta Metall. 20 (1972) 887.
[11] B. Feng, Y.C. Xin, R. Hong, H.H. Yu, Y. Wu, Q. Liu, Scr. Mater. 98 (2015) 56.
[12] Y. Brechet, J.D. Embury, Scr. Mater. 68 (2013) 1.
[13] L. Thilly, F. Lecouturier, G. Coffe, J.P. Peyrade, S. Askenazy, IEEE Trans. Appl. Supercond. 10 (2000) 1269.
[14] R.W. Ure, R.R. Heikes, Thermoelectricity: Science and Engineering, Interscience Publishers, Inc., New York – London (1961), p. 458.
[15] S. Vives, P. Bellanger, S. Gorsse, C. Wei, Q. Zhang, J.-C. Zhao, Chem. Mater. 26 (2014) 4334.
[16] S. Muntyanu, E.B. Sokolov, E.S. Makarov, Izv. Akada Nauk SSSR, Neorgan. Mater. 2 (1966) 870.
[17] E.N. Nikitin, Izv. Akada Nauk SSSR, Neogran. Mater. 4 (1968) 1902.
[18] I.-H. Jung, D.-H. Kang, W.-J. Park, N.J. Kim, S. Ahn, Calphad-Comput. Coupling Phase Diagrams Thermochem. 31 (2007) 192.
[19] A. Kozlov, J. Groebner, R. Schmid-Fetzer, J. Alloy. Compd. 509 (2011) 3326.
[20] J.S. Kirkaldy, L.C. Brown, Can. Metall. Q. 2 (1963) 89.